Biochimica et Biophysica Acta, 983 (1989) 241–246
Elsevier

BBAMEM 74494

Neutron and X-ray diffraction structural analysis of phosphatidylinositol bilayers

Robert V. McDaniel [1,*] and Thomas J. McIntosh [2]

[1] *Department of Physiology and Biophysics, State University of New York, Stony Brook, NY and* [2] *Department of Cell Biology, Duke University Medical Center, Durham, NC (U.S.A.)*

(Received 27 January 1989)

Key words: Phosphatidylinositol bilayer; Bilayer; Osmotic pressure; Lamellar repeat period; Neutron diffraction; X-ray diffraction

Phosphatidylinositol (PI) bilayers, squeezed together by applied osmotic pressures, were studied by both neutron diffraction and X-ray diffraction. The lamellar repeat period for PI bilayers decreased from 9.5 nm at an applied pressure of $1.1 \cdot 10^6$ dyn/cm^2 (1.1 atm) to 5.4 nm at an applied pressure of $1.6 \cdot 10^7$ dyn/cm^2 (16 atm). Further increases in applied pressure, up to $2.7 \cdot 10^9$ dyn/cm^2 (2700 atm) reduced the repeat period by only about 0.3 nm, to 5.1 nm. Thus, a plot of applied pressure versus repeat period shows a sharp upward break for repeat periods less than about 5.4 nm. For repeat periods of less than 5.4 nm, analysis of neutron-scattering density profiles and electron-density profiles indicates that the structure of the PI bilayers changes as the bilayers are dehydrated, even though there are only small changes in the repeat period. These structural changes are most likely due to removal of water from the headgroup regions of the bilayer. D_2O/H_2O exchange experiments show that, at an applied pressure of $2.8 \cdot 10^7$ dyn/cm^2, water is located between adjacent PI headgroups in the plane of the bilayer. We conclude that, although electrostatics provide the dominant long-range repulsive interaction, hydration repulsion and steric hindrance between PI headgroups from apposing bilayers provide the major barriers for the close approach of adjacent PI bilayers for repeat periods less than 5.4 nm. This structural analysis also indicates that the phosphoinositol group extends from the plane of the bilayer into the fluid space between adjacent bilayers. This extended orientation for the headgroup is consistent with electrophoretic measurements on PI vesicles.

Introduction

PI, or monophosphoinositide, is a negatively charged lipid found in many plasma membranes. This lipid is of particular interest for several reasons. First, monophosphoinositide, along with the polyphosphoinositides, plays an important role in the agonist-induced formation of the second messengers diacylglycerol and inositol trisphosphate [1,2]. The regulation of the 'phosphoinositide response' is the subject of much recent biochemical research [3–7]. Second, several proteins, including hydrolytic enzymes, antigens, and cell adhesion molecules, are anchored to the membrane by glycosyl-phosphatidylinositol linkages [8–11]. Third, the orientation of PI headgroup may be a factor in the fusion of lipid vesicles [12].

Bilayer membranes formed from PI have been investigated by several physical techniques, including nuclear magnetic resonance [13], electron spin resonance [14,15], electrophoresis [16], metachromatic dye adsorption [14], analytical ultracentrifugation [17] and electron microscopy [15,16]. These studies have been primarily concerned with the distribution of PI in vesicles. Although Sugiura [18] has analyzed 1-(3-*sn*-phosphatidyl)-L-*myo*-inositol-3,4-bisphosphate/water systems by X-ray diffraction techniques, there has been relatively little work done on the structure of PI bilayers. Such structural information could be critical to an understanding at the molecular level of the various roles of PI in biological membranes.

In this paper, we investigate by both neutron and X-ray diffraction techniques the organization of PI bilayers squeezed together by applied osmotic pressure.

Materials and Methods

The sodium salt of PI from bovine liver was purchased from Avanti Polar lipids, Inc. The lipid showed a single spot on thin-layer chromatograms (oxalate silica gel

* Present Address: 7 Scott Drive, Melville, NY 11747, U.S.A.

Abbreviations: PI, phosphatidylinositol; PVP, poly(vinylpyrrolidone); PC, phosphatidylcholine.

Correspondence: T.J. McIntosh, Department of Cell Biology, Duke University Medical Center, Durham, NC 27710, U.S.A.

0005-2736/89/$03.50 © 1989 Elsevier Science Publishers B.V. (Biomedical Division)

plates) with a solvent system of chloroform/methanol/water (65 : 25 : 4, v/v).

Neutron-diffraction experiments were performed at the High Flux Beam Reactor H-3B crystallography station [19] at Brookhaven National Laboratories. Specimens were prepared by drying a chloroform solution containing 10–20 mg of lipids onto acid-cleaned 1 mm thick quartz microscope slides. A razor blade was used to trim the edges of the dried lipid film to final dimensions of 40 mm × 15 mm. After 12 h equilibration with the atmosphere above a saturated aqueous KCl solution at 11°C, the quartz slide was mounted in a sealed aluminum chamber containing a vial of saturated salt solution at 21.3°C. The temperature was controlled to within 0.05 C° by use of a water bath. The relative vapor pressure (p/p_0) was held constant within the chamber with saturated aqueous salt solutions [20,21]. The following saturated salt solutions were used to obtain the relative vapor pressures indicated in parentheses: K_2SO_4 (0.98), $NaSO_4$ (0.93), KCl (0.86), NH_4Cl (0.80), NaCl (0.76), $NaNO_2$ (0.66), $CaCl_2$ (0.32), $KC_2H_3O_2$ (0.20), and LiCl (0.15). In these controlled humidity atmospheres, the pressure applied to the specimen is given by

$$P = -(RT/V_w)\ln(p/p_0)$$

where R is the molar gas constant, T is the temperature, and V_w is the molar volume of water [22]. To ensure that the observed structure amplitudes were on the same relative scale, the same specimen, specimen geometry, and data collection time were used in the neutron diffraction experiments. The incident neutron beam was 4 mm in diameter and intersected the 40 mm long lipid film as an ellipse. The quartz slide was rotated over a 10° angle (increments of 0.1°) relative to the beam axis. Therefore the major axis of this ellipse varied as the sin of the rotation angle, leading to a geometrical correction of $s \approx (h/d)$ for the diffracted intensity of order h, where d is the lamellar repeat period [23]. Another factor of s arose from the Lorentz correction [24], so that the measured intensities were corrected by multiplying them by $s^2 = (h/d)^2$. Entire elliptical reflections were collected on a two-dimensional position-sensitive gas flow detector. The integration and background subtraction procedures have been described in detail previously [19]. D_2O/H_2O exchange was performed at a partial pressure of 0.98, by the use of a saturated salt solution of K_2SO_4 in a mixture of D_2O and H_2O (20 vol% D_2O).

X-ray diffraction experiments were performed both on oriented samples in controlled humidity atmospheres and on unoriented suspensions. The oriented specimens were prepared in a similar manner to those described above for the neutron experiments, except that the specimen was dried from an aqueous suspension onto a flat sheet of aluminum foil. The aluminum foil was then given a convex curvature and mounted in a humidity chamber on a line-focused single-mirror X-ray camera. Unoriented suspensions were prepared by adding water solutions of PVP (Sigma Chemical Co.) to dry PI and allowing the suspension to incubate for several hours. The osmotic pressures of various PVP/water solutions have been calculated [25] from the virial coefficients of Vink [26]. The PI suspensions were sealed in quartz glass capillary tubes and mounted in a pinhole collimation X-ray camera containing three or more sheets of Kodak DEF-5 X-ray film in a flat plate film cassette. For both oriented and unoriented specimens, the specimen-to-film distance was 10 cm, and exposure times were of the order of 5–15 h. The films were processed by standard techniques and densitometered with a Joyce-Loebl Model MKIIIC microdensitometer as described previously [27]. For the unoriented specimen, the intensities were corrected by multiplying by a factor of h^2, whereas for the oriented specimens a single factor of h was used. The validity of these correction factors has previously been demonstrated [27]. Structure factors from different X-ray diffraction experiments were normalized by the procedure of Blaurock [28].

Results

For oriented PI specimens, both neutron and X-ray diffraction patterns contained four reflections which indexed as orders of a lamellar repeat period. Over the entire range of relative vapor pressures used ($p/p_0 = 0.15$ to $p/p_0 = 0.98$, which correspond to applied pressures of $P = 2.7 \cdot 10^9$ dyn/cm^2 to $P = 2.8 \cdot 10^7$ dyn/cm^2), the lamellar repeat period varied from a minimum of 5.06 nm to a maximum of 5.28 nm. For the unoriented PI suspensions, the lamellar repeat period ranged from 5.14 nm in 60% PVP (which corresponds to an applied osmotic pressure of $P = 5.8 \cdot 10^7$ dyn/cm^2)

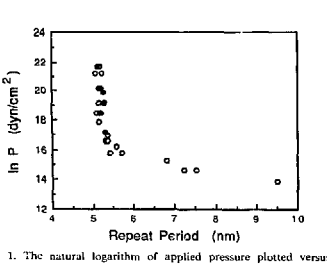

Fig. 1. The natural logarithm of applied pressure plotted versus lamellar repeat period for PI bilayers in neutron diffraction (●) and X-ray diffraction (○) experiments.

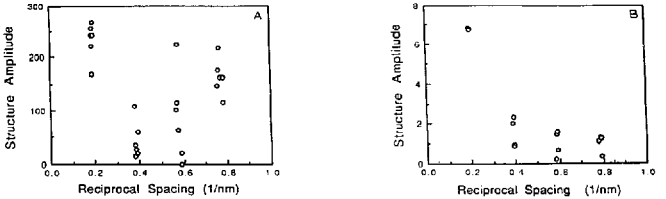

Fig. 2. Observed structure amplitudes for PI bilayers plotted versus reciprocal space coordinate in (A) neutron diffraction and (B) X-ray diffraction experiments. Structure amplitudes are shown for four lamellar orders of diffraction for repeat periods ranging from 5.28 to 5.06 nm.

to 9.50 nm in 15% PVP (which corresponds to an applied osmotic pressure of $1.1 \cdot 10^6$ dyn/cm^2). In lower concentrations of PVP no discrete reflections were observed, presumably because the fluid spaces between bilayers became large and irregular in width. Four orders of diffraction were recorded for PI in 50% and 60% PVP, whereas only two orders were recorded for PVP concentrations between 15% and 40% PVP. A plot of the natural logarithm of applied pressure ($\ln P$) versus lamellar repeat period (d) is shown in Fig. 1 for all of the oriented and unoriented specimens. The plot has two distinct regions. For applied pressures in the range $22 < \ln P < 16$, the repeat period varies only by about 0.3 nm. However, as the applied pressure decreases from $\ln P = 16$ to $\ln P = 13.9$, the lamellar repeat period increases by over 4 nm.

Even though the repeat period changes by only a few tenths of a nm for applied pressures in the range $22 < \ln P < 16$, there are large differences in the observed intensity distributions. Figs. 2A and 2B show plots of the structure amplitudes of the first four orders of diffraction over this range of applied pressure for the neutron and X-ray experiments, respectively. It can be seen that for both neutron and X-ray diffraction patterns, the structure amplitude for each diffraction order varies considerably with relatively small changes in repeat period. This observation indicates that, over this range of applied pressure, the structure of the bilayer changes as the applied pressure is increased [29].

For the neutron diffraction data, phase angles were determined for each diffraction order by the use of D_2O/H_2O exchange [30]. D_2O has a higher neutron-scattering length density than does H_2O, and since water is primarily localized on the outer edges of the unit cell (in the fluid spaces between membranes and in the lipid head group regions), D_2O/H_2O exchange changes the magnitude of the structure factors in a predictable manner when the correct phase combination is obtained [23,30,31]. For centrosymmetric systems, such as these PI bilayers, each phase angle must be either 0 or π. To determine the phase angle for each reflection we have used the procedure of Hargreaves [32], in a manner similar to that of Zaccai et al. [31]. Consider a fluid space of width w centered at the origin between adjacent bilayers. In a D_2O/H_2O exchange, the difference between structure factors in the presence of D_2O and H_2O is given by

$$\exp(i\alpha_D(h))|F_D(h)| - \exp(i\alpha_H(h))|F_H(h)|$$
$$= (2/h\pi)(\rho_D - \rho_H)\sin(\pi hw/d)$$

where $|F(h)|$ are the structure amplitudes for order h, $\alpha(h)$ are the phase angles for order h, ρ is the neutron scattering density, and the subscripts H and D refer to H_2O and D_2O, respectively [31]. Thus, since $\rho_D > \rho_H$, a plot of $A(h) = h[\exp(i\alpha_D(h))|F_D(h)|]/\sin(\pi hw/d)$ versus $B(h) = h[\exp(i\alpha_H(h))|F_H(h)|]/\sin(\pi hw/d)$ should yield a straight line with a slope of $+1.0$ and a positive intercept with the $A(h)$ axis, provided the correct phase combination is selected. Following the procedure of Zaccai et al. [31], we set $w = 1.0$ nm. A plot of $A(h)$ versus $B(h)$ is shown in Fig. 3 for a phase combination of 0, π, π, π, for PI in H_2O and 0, 0, π, and π for PI in D_2O. This phase combination gives a straight line (least-squares fit of $r^2 = 0.98$) with a posi-

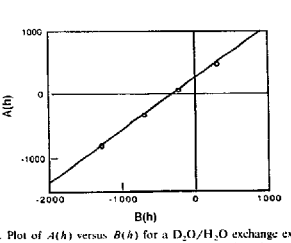

Fig. 3. Plot of $A(h)$ versus $B(h)$ for a D_2O/H_2O exchange experiment. The straight line is the least-squares fit to the four data points. See text for details.

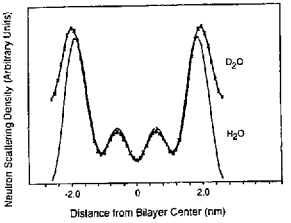

Fig. 4. Neutron-scattering density profiles for PI at a relative vapor pressure of 0.98 for H_2O and 20 vol% D_2O.

tive slope and a positive y intercept. This indicates that this is the correct phase combination. This sequence of phase angles is the same as that of PC under similar experimental conditions [23,31].

Neutron density profiles for PI in H_2O and 20 vol% D_2O are shown in Fig. 4. In these profiles, the origin has been shifted to the geometric center of the bilayer by changing the phases of the odd orders of diffraction by 180°. Thus, the low-density trough in the geometric center of the bilayer (0 nm) corresponds to the localization of the terminal methyl groups of the lipid hydrocarbon chains and the two highest-density peaks correspond to the lipid polar headgroups. The medium-density regions between the headgroup peaks and the terminal methyl trough correspond to the lipid methylene chains. Replacement of H_2O with D_2O increases the neutron density in the hydrated polar regions at the edges of the profile, but has no significant effect on the hydrocarbon region of the bilayer.

Fig. 5 shows neutron-scattering amplitude density profiles in H_2O at partial vapor pressures of 0.98, 0.76 and 0.15. Each of these profiles is similar in shape, but the profiles differ in some significant details. First, the distance between headgroup peaks across the bilayers increases slightly as the partial vapor pressure decreases; the peak-to-peak distance is 3.73 nm at $p/p_0 = 0.98$, 3.90 nm at $p/p_0 = 0.76$ and 3.92 at $p/p_0 = 0.15$. Second, the terminal methyl trough becomes deeper as the partial vapor pressure decreases. Third, the neutron density at the outer edge of each profile increases relative to the average density of the profile with decreasing partial vapor pressure. Similar structural changes have been observed for dioleoyl PC bilayers for relative vapor pressure between 0.98 and 0.66 [23].

Based on the similarity of the neutron-scattering amplitude density profiles for PI (Fig. 5) and PC [32], we have used the same phase angles for the X-ray reflections for PI as have been determined for PC [25,33]. This was also the same phase angle combination

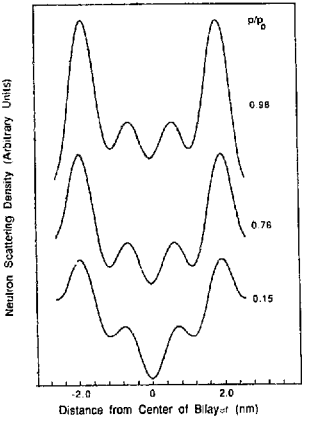

Fig. 5. Neutron-scattering density profiles of PI bilayers at relative vapor pressures of 0.98, 0.76 and 0.15.

as used for 1-(3-*sn*-phosphatidyl)-L-*myo*-inositol 3,4-bisphosphate bilayers [18]. Electron density profiles for PI at partial vapor pressures of 0.93, 0.66 and 0.32 are shown in Fig. 6. The electron density profiles (Fig. 6) are somewhat different in shape from the neutron-scattering amplitude profiles (Fig. 5), presumably be-

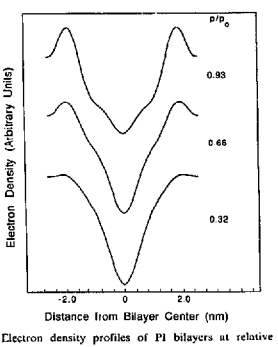

Fig. 6. Electron density profiles of PI bilayers at relative vapor pressures of 0.93, 0.66 and 0.32.

cause of the different scattering-length densities to neutrons and X-rays [34] for the H, C, O, and P atoms in the PI bilayers. As in the neutron-scattering amplitude profiles, each electron density profile contains two high-density headgroup peaks on either side of a low-electron density hydrocarbon chain region at the center of the bilayer. The shape of the profile and distance between the headgroup peaks are both a function of the partial vapor pressure. The distance between headgroup peaks across the bilayer increases slightly from about 3.8 nm, at a relative vapor pressure of 0.93, to about 4.1 nm, at a relative vapor pressure of 0.32, where the headgroup peaks from adjacent bilayers are barely resolved.

Discussion

The neutron diffraction and X-ray diffraction data presented in this paper provide information on the structure of PI bilayers and the interaction between apposing bilayer surfaces. First, let us consider the pressure/repeat period data presented in Fig. 1. As the applied pressure is reduced from $\ln P = 16$ to $\ln P = 14$, the lamellar repeat period increases by about 4 nm. This increase in repeat period is undoubtedly due primarily to electrostatic repulsion between the charged PI bilayers [35–37]. The sharp upward break in the plot of $\ln P$ versus repeat period (Fig. 1) observed at $\ln P > 16$, indicates the presence of at least one additional short-range repulsive pressure. Two possible short-range pressures that have been observed for PC membranes are hydration pressure [22,25,38,39] and a pressure arising from steric interactions between headgroups from apposing bilayers [27]. It is likely that both hydration and steric pressures contribute to $\ln P > 16$. Cowley et al. [35] have presented data which show the influence of hydration repulsion on PC bilayers containing 10 mol% PI. The results we have obtained do not provide enough information to separate the contributions of the hydration and steric pressures or determine the magnitude of each of these pressures. However, the structural data discussed below argue that steric hindrance between apposing headgroups provides at least some of the observed short-range repulsion.

For the range of applied pressures $13 < \ln P < 17$, the X-ray data are not of high enough resolution to determine the bilayer structure. However, both the neutron diffraction and X-ray diffraction data indicate that as the PI bilayers are squeezed close together by higher applied pressures ($\ln P > 17$) structural changes occur in the bilayer. Neutron-scattering density profiles (Fig. 5) and electron density profiles (Fig. 6) show that three structural changes occur as pressure is increased above $\ln P = 17$: (1) the distance between headgroup peaks across the bilayer becomes progressively larger, (2) the terminal methyl trough in the center of the bilayer becomes more pronounced, and (3) the density at the outer edges of the profile increases. The most likely explanation for these observations is that at these pressures, apposing membranes come into contact and that water is being removed from the headgroup region of the bilayer. The D_2O/H_2O exchange experiments (Fig. 4) clearly show, at a relative vapor pressure of 0.98 ($\ln P = 17$), that water penetrates well into the lipid headgroup region. The removal of some of these water molecules would decrease the area per lipid molecule and therefore increase the bilayer thickness, assuming the lipid bilayer is volumetrically incompressible [22]. The increase in bilayer thickness corresponds to a straightening or ordering of the lipid hydrocarbon chains. This results in a closer registration of the terminal methyl groups in the bilayer center, and therefore, a deeper central trough in the profiles (Figs. 5 and 6). For equivalent pressures, similar structural changes have been observed for PC bilayers [23,27]. In the case of PC bilayers, it was demonstrated that these structural changes coincided with the onset of steric hindrance between adjacent bilayers [27]. That is, for PC bilayers, only relatively small structural changes occur for pressures in the range $13 < \ln P < 17$, where water is removed primarily from the fluid spaces between adjacent bilayers [25,27,40]. However, as the applied pressure is increased from $\ln P = 17$ to $\ln P = 21$, for both PC [27] and PI (Figs. 5 and 6), measurable structural changes changes occur, most likely due to removal of water from the bilayer headgroup region. The increased density at the outer edges of the bilayer at the highest applied pressures (Figs. 5 and 6) is consistent with the apposing bilayers coming into contact. That is, when enough water is removed so that the inositol groups from apposing bilayers come together, the concentration of inositol groups in the interbilayer space increases. This causes an increase in density at the outer edges of the profiles.

At a relative vapor pressure of 0.93, the distance between headgroup peaks in the electron density profiles is about 3.8 nm. This is very similar to the peak-to-peak separation observed in egg PC bilayers at the same relative vapor pressure [27]. The headgroup peak in electron density profiles is located near the center of mass of the headgroup, that is between the phosphate moiety and the glycerol backbone. (In the neutron-scattering density profiles the headgroup peak is somewhat closer to the glycerol backbone due to the the relatively large neutron scattering density of the lipid carbonyl groups [41]). Space-filling models of PI show that if the headgroup were fully extended, the inositol group would extend about 0.7–1.0 nm beyond the headgroup peak in the electron density profiles into the fluid space between adjacent bilayers. This means that if the PI headgroups were fully extended, the total thickness of a PI bilayer would be about 5.2–5.8 nm.

Thus, steric interaction between headgroups from apposing bilayers would be expected at these repeat periods if the PI headgroup were fully extended. The onset of steric hindrance would occur at smaller repeat periods if the PI headgroups were not fully extended. Our profiles (Figs. 5 and 6) are not of high enough resolution to determine the precise headgroup orientation or provide information on possible changes in headgroup conformation during dehydration. However, the break in the plot of ln P versus repeat period (Fig. 1) begins at repeat period of about 5.4–5.6 nm, in the range of repeat periods where steric interactions would occur if the phosphoinositol groups extended from the plane of the bilayer surface.

The idea that the PI headgroups extend from the bilayer and cause steric hindrance to the close approach of adjacent bilayers is consistent with the work of Sundler and Papahadjopoulos [12], who have shown that the presence of PI inhibits the calcium-induced fusion of phosphatidate vesicles. They have suggested that the bulky hydrated phosphoinositol headgroup might inhibit bilayer fusion by not allowing the formation of a complex between phosphate groups from apposing membranes [12]. The bulky PI headgroup might also effect the electrophoretic mobility of vesicles containing PI. For example, the electrophoretic mobility of PI vesicles [16,42] is smaller than that of vesicles formed from phosphatidylglycerol, or phosphatidylserine [42,43]. This can be qualitatively explained by the hydrodynamic drag exerted by the phosphoinositol group, which would reduce the electrophoretic mobility of PI vesicles as compared to other charged phospholipid vesicles [44].

Acknowledgements

This work was supported by NIH Grant GM-27278 (to T.J.M.) and by NIH grants to Dr. S. McLaughlin. The research at Brookhaven National Laboratory was carried out under the auspices of the U.S. Department of Energy with the kind assistance of Dr. Benno Schoenborn, Dr. Anand Saxena, and Dr. Jurg Schaefer. We thank Dr. Glenn King for the use of his sample holder.

References

1 Berridge, M.J. (1984) Biochem. J. 220, 345–360.
2 Michell, R.H. (1979) Trends Biochem. Sci. 4, 128–131.
3 Baraban, J.M., Snyder, S.H. and Alger, B.E. (1985) Proc. Natl. Acad. Sci. USA 82, 2538–2542.
4 Streb, H., Bayerdorfer, E., Haase, W., Irvine, R.F. and Schulz, I. (1984) J. Membr. Biol. 81, 241–253.
5 Michaelson, D.M., Horowitz, A.F. and Klein, M.P. (1973) Biochemistry 12, 2637–2645.
6 Baker, P.F. and Whitaker, M.J. (1978) Nature 276, 513–515.
7 Wilson, D.B., Bross, T.E., Sherman, W.R., Berger, R.A. and Majerus, P. (1985) Proc. Natl. Acad. Sci. USA 82, 4013–4017.
8 Romero, G. (1988) Science 240, 509–511.
9 Low, M.G. and Saltiel, A.R. (1988) Science 239, 268–275.
10 Sefton, B.M. and Buss, J.E. (1987) J. Cell Biol. 104, 1449–1453.
11 Caras, I.W., Weddell, G.N., Davitz, M.A., Nussenweig, V. and Martin, D.W. (1987) Science 238, 1280–1283.
12 Sundler, R. and Papahadjopoulos, D. (1981) Biochim. Biophys. Acta 649, 751–758.
13 Berden, J.A., Barker, R.W. and Radda, G.K. (1975) Biochim. Biophys. Acta 75, 186–208.
14 Massari, S., Pascolini, D. and Gradenigo, G. (1978) Biochemistry 17, 4465–4469.
15 Ohki, K., Sekiya, T., Yamauchi, T. and Nozawa, Y. (1981) Biochim. Biophys. Acta 644, 165–174.
16 Hammond, K., Reboiras, M.D., Lyle, I.G. and Jones, M.N. (1984) Biochim. Biophys. Acta 774, 19–25.
17 Litman, B.J. (1973) Biochemistry 12, 2545–2554.
18 Sugiura, Y. (1981) Biochim. Biophys. Acta 641, 148–159.
19 Schoenborn, B. (1984) in Neutrons in Biology (Schoenborn, B., ed.), pp. 261–280, Plenum Press, New York.
20 O'Brien, F.E.M. (1948) J. Sci. Instrum. 25, 73–76.
21 Weast, R.C. (1984), Handbook of Chemistry and Physics, CRC Press, Boca Raton Florida.
22 Parsegian, V.A., Fuller, N. and Rand, R.P. (1979) Proc. Natl. Acad. Sci. USA 76, 2750–2754.
23 King, G.I., Chao, N.M. and White, S.H. (1984) in Neutrons in Biology (Schoenborn, B., ed.), pp. 159–172, Plenum Press, New York.
24 Saxena, A.M. and Schoenborn, B. (1977) Acta Cryst. A33, 813–818.
25 McIntosh, T.J. and Simon, S.A. (1986) Biochemistry 25, 4058–4066.
26 Vink, H. (1971) Eur. Polym. J. 7, 1411–1419.
27 McIntosh, T.J., Magid, A.D. and Simon, S.A. (1987) Biochemistry 26, 7325–7332.
28 Blaurock, A.E. (1971) J. Mol. Biol. 56, 35–52.
29 Worthington, C.R., King, G.I. and McIntosh, T.J. (1973) Biophys. J. 13, 480–494.
30 Blasie, J.K., Schoenborn, B. and Zaccai, G. (1975) in Neutron Scattering for the Analysis of Biological Structures (Schoenborn, B.P., ed.), pp. III58–III67, Brookhaven National Laboratory, Upton, New York.
31 Zaccai, G., Blasie, J.K. and Schoenborn, B.P. (1975) Proc. Natl. Acad. Sci. USA 72, 376–380.
32 Stout, G. and Jensen, L. (1968). X-ray Structure Determination, Macmillan, New York.
33 Torbet, J. and Wilkins, M.H.F. (1976) J. Mol. Biol. 62, 447–458.
34 Schoenborn, B.P. (1975) in Neutron Scattering for the Analysis of Biological Structures (Schoenborn, B.P., ed.), pp. 110–117, Brookhaven National Laboratory, Upton, New York.
35 Cowley, A.C., Fuller, N.L., Rand, R.P. and Parsegian, V.A. (1978) Biochemistry 17, 3163–3168.
36 Loosley-Millman, M.E., Rand, R.P. and Parsegian, V.A. (1982) Biophys. J. 40, 221–232.
37 Marra, J. (1986) Biophys. J. 50, 815–825.
38 LeNeveu, D.M., Rand, R.P., Parsegian, V.A. and Gingell, D. (1977) Biophys. J. 18, 209–230.
39 Lis, L.J., McAlister, M., Fuller, N., Rand, R.P. and Parsegian, V.A. (1982) Biophysical J. 37, 657–666.
40 Simon, S.A., McIntosh, T.J. and Magid, A.D. (1988) J. Colloid Interface Sci. 126, 74–83.
41 Worcester, D.L. and Franks, N.P. (1976) J. Mol. Biol. 100, 359–378.
42 Eisenberg, M., Gresalfi, T., Riccio, T. and McLaughlin, S. (1979) Biochemistry 18, 5213–5223.
43 Lau, A., McLaughlin, A. and McLaughlin, S. (1981) Biochim. Biophys. Acta 645, 279–292.
44 McDaniel, R.V., McLaughlin, A., Winiski, A., Eisenberg, M. and McLaughlin, S. (1984) Biochemistry 23, 4618–4623.